Chapter 2
Morphological Aspects of Fatigue Crack Formation and Growth

2.1 Introduction

The aim of this chapter is at providing some elementary information about the various fatigue mechanisms that can take place in the materials that is an essential background for the study of fatigue and the comprehension of what may have been happened in a work piece that failed by fatigue and why it failed. What has been shown in the previous chapter is that any single cycle of fatigue is introducing in the material a sub-microscopic damage in a single grain or better within a single persistent slip line in the form of a sub-microscopic cavity (see Sect. 1.4, Fig. 1.43) that may grow to a finite extension resulting in a macro crack. A macro crack produced by slip band formation is something not visible at naked eye since it can be just 300 µm long (see Figs. 1.57 and 1.66). When this macro crack grows at each applied fatigue cycle it leaves on the fracture surface a characteristic feature that can be detected. Therefore, a very important tool given to designer, alas too often forgotten, is the *post mortem* examination of failed piece. On the fracture surface is written the complete story of its destiny. What is actually needed is the key to decode and interpreter the characteristic features that we may see at naked eye and, above all, those we cannot see at naked eye, but with sophisticated tools such as high definition optical microscope and scanning electron microscope (SEM), in particular. Dough today engineers know by general line what is a SEM and its applications, it may be convenient to spend few words. Electrons may go beyond what can be seen with visible light (optical microscopy). However, electrons can be transmitted through a few hundreds to a thousand Ångstroms of metal. Therefore, fracture surface cannot be examined directly by a transmission electron microscope (TEM). Because of that, it is necessary to transfer the microscopic features we want to see to a thin, electron-transparent replica. This is done by covering the surface under investigation with a liquid plastic material. This liquid will enter any tiny detail of the wetted surface that will remain imprinted on the plastic when it hardens. After hardening, the plastic is stripped very carefully from the mating surface.

The next step is to place the plastic replica in a vacuum chamber where a thin layer of carbon is deposited by evaporation of a pair of carbon electrode. Some heavy metal, such as gold or platinum, can be used instead, which will enhance contrast. At this point, the plastic is dissolved in acetone and the carbon replica remains, which has kept all details of the original surface. The replica is too thin to have any strength so that it is recovered on a copper grid of about 80–100 μm spacing that becomes its support any time it is needed to handle it. It is obvious that the original surface details will remain on the carbon replica upside down, so that valleys will appear like dimples and holes like protruding. With the introduction of the scanning electron microscope it has become possible to observe the fracture surface or the surface of the work piece directly. A high intensity electron beam of small diameter scans across the surface. Due to the excitation of these primary electrons, secondary electrons are emitted by the target surface. These secondary electrons produce an image of the surface under investigation which can be made visible on a cathode-ray oscilloscope scanning at the same rate as the electron beam. In Chap. 1 some examples of optical microscopy and SEM as well have been shown. Exemplary is the Ewing and Humphrey optical examination already in 1903 of the surface of a fatigue specimen (see Fig. 1.38) that can be considered archetypal. Modern, advanced fatigue design cannot skip over the instrumental aspect and be confined to calculus, even though today designers may dispose of very advanced computer codes. Structures and components still fail, though computer designed. Materials and component behavior often do not comply with computer schematization. It is fundamental to understand why failed and in this effort optical and electron microscopy play a fundamental role. This Chapter is aiming at providing a little bit of that knowledge.

2.2 Extrusions and Intrusions

It has been said in Sect. 1.4 that in high cycle fatigue initial damage nucleates in some surface grains along persistent slip bands in the form of pores or submicroscopic cracks. In those bands plastic deformation concentrates and slip is an irreversible process due to damage. Slips are initiated by resolved shearing stress reaching the critical value $\tau_{r,cr}$ just in some grains on the surface (see Fig. 1.35) where plain stress conditions prevail. There are several models describing the micro crack formation in slip lines. Interesting is the model proposed by Neumann [1] and schematized in Fig. 2.1. According to this model, during the traction phase of the cyclic stress, Fig. 2.1a, a dislocation source is activated and slip occurs along a preferential direction 1 on a crystallographic plane. A submicroscopic discontinuity is then formed that influence another source of dislocation and a new slip takes place along line 2 perpendicular to the first (intersecting slip), Fig. 2.1b. When load is inverted, both planes 1 and 2 are activated, but in the opposite direction living the surface in the condition depicted in Fig. 2.1c. Apparently, the surface has returned in the initial condition and the indentation disappeared, but the two faces that for a

Fig. 2.1 Neumann model of micro crack formation during fatigue cycling [1]
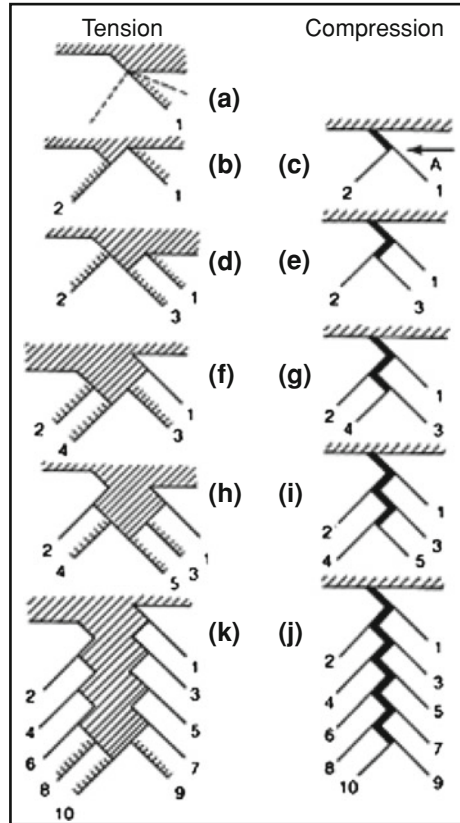
while have been exposed to air oxidase, though very lightly, but this is enough to prevent surface re-cohesion and a damage remains indicated by arrow A in Fig. 2.1c. This let us believe that fatigue in vacuum must not exist. This is partially true in that fatigue in vacuum is effectively much less damaging than in dry air (see Fig. 2.45), but not completely true since slips are the consequence of a plastic deformation that is not totally recoverable. Slips are, therefore, irreversible in nature and damage cannot heal. The repetition of tension–compression cycles leads to the activation of new slip planes, always in the same slip system, with the result of generating a continuous path along which damage generates and accumulates and eventually becomes a micro crack Fig. 2.1d through 2.1j. It worth noting that according to this model the micro crack, though advancing locally in a zigzag mode (see Figs. 1.64 and 1.65), is actually proceeding in a direction perpendicular to external loads. Another mechanism particularly important is the one that leads to the extrusion-intrusion formation. An extrusion is a metal lamina extremely thin that is extruded from the surface of a slip band. This is shown in Fig. 2.2 according to Forsyth [2]. Extrusion formation is a typical consequence of dislocation movements during fatigue. Because extrusions are normally accompanied by
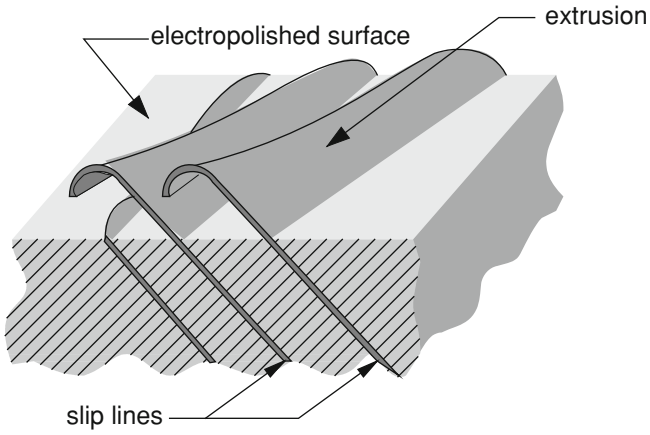
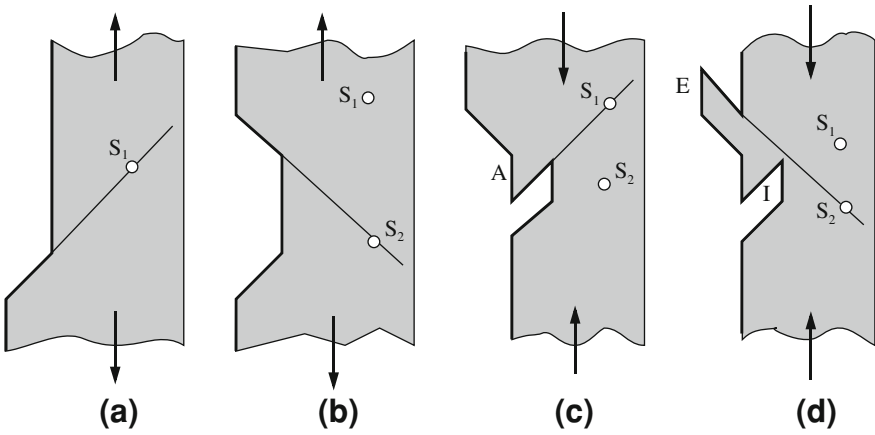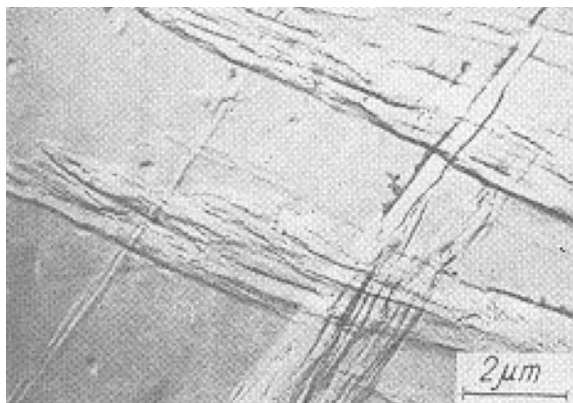**Fig. 2.2** Schematic of extrusions in copper according to Forsyth

Fig. 2.3 Schematic of extrusion intrusion formation according to Cottrell and Hull

Fig. 2.4 Evidence of intersecting slip bands and cross slip in an Armco iron [10]
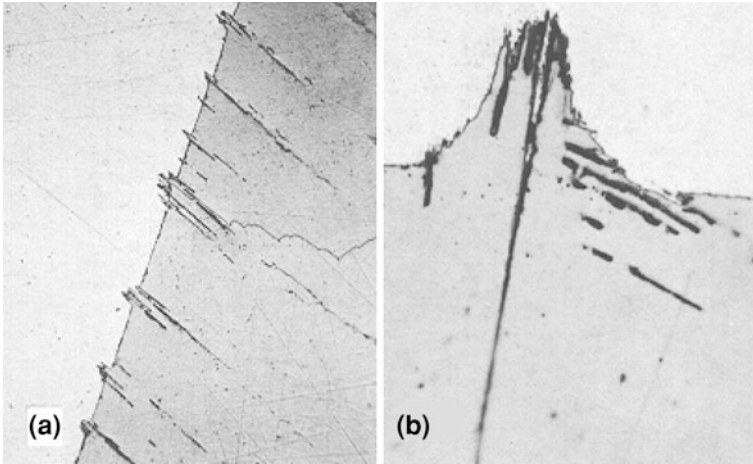
Fig. 2.5 Extrusions observed in **a** a copper specimen and in **b** Fe-3 Si [12]

cracks in the slip packet, they may be of significance in crack initiation. Intrusions are the inverse of extrusions and are narrow and shallow crevices. These surface discontinuities are approximately 10^{-4}–10^{-5} cm in height and appear as early as some percent of the total life of a specimen. Forsyth first [2] and Forsyth and Stubbington [3–6] report the extrusions formation on the surface of a $4\frac{1}{2}$ Cu-aluminum specimen cold-working hardened in which slip lines were very fine. They were no thicker than 0.1 and about 10 μm long. Micro cracks were also present. At −196 °C they disappeared, but not the slip bands that became coarse. Also in 10 % Zn-aluminum alloys they appeared, but this time also at −196 °C. The presence of extrusion has been reported also in carbon steels [7] and hardened steels [8]. Cottrell and Hull [9] gave an interpretation of extrusions formation in FCC metals expanding the model of slips and slip bands already seen in Fig. 1.42. Their model is shown in Fig. 2.3. In the new scheme two slip lines are interested that are perpendicular to each other. At the beginning an edge dislocation source S_1 is activated and the crystal slips along the corresponding plane and direction. This leaves the surface of the material in the form shown in Fig. 2.3a. Successively, but always in the same traction phase, a second source S_2 is activated having a slip plane at 45° with the external load, but perpendicular to the former plane (intersecting slips). The new appearance of the external surface is shown in Fig. 2.3b. Note that in such a sliding the first slip plane moves upward relative to its original position. This makes it happen that in the successive phase of unloading when source S_1 on plane 1 is reactivated it creates a tooth A that in turn breaks the slip plane of source S_2, as it can be seen in Fig. 2.3c. When this second source is reactivated, during unloading, the surface has the appearance of Fig. 2.3d where the extrusion E and the intrusion I are formed. Figure 2.4 [10] shows an example of intersecting slip lines grouped in bands with cross slip. Without load inversion and consequent inversion of dislocation motion extrusions would not appear. A model
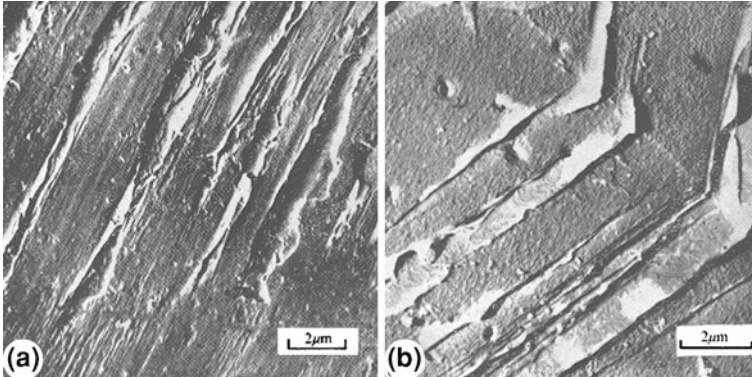
Fig. 2.6 Extrusions formation in copper under low cycle fatigue [9]

of extrusion-intrusion formation activated by screw dislocations was proposed by
Mott [11]. An example of extrusion in copper and Fe-3 Si is offered in Fig. 2.5 [12].
Note that there is a difference in the appearance of slip bands in copper and Fe-3 Si.
Copper exhibits wavy glide while Fe-3 Si exhibits more planar glide (see Fig. 1.44).
Alloys of low stacking fault energy, such as Cu-7 Al, also develop slip bands that
resemble those in Fe-3 Si rather than those in copper. It can be seen the loss of
surface smoothness and the crack formation associated with extrusions. Another
example of extensive extrusions formation in copper under low cycle fatigue can be
seen in Fig. 2.6 [9].

2.3 Morphology of Crack Propagation

From a phenomenological point of view Stage I of fatigue can be described as a
back and forth slip on a series of contiguous crystallographic plane to form a band
(see Fig. 1.42). Bands so formed have, generally, height of the order of many
hundreds of Angstrom. It is within this slip bands that the process of pores
nucleation and coalescence, already described in the previous paragraphs, develop.
The process eventually leads to micro cracks formation. Often, extrusion and
intrusions may also appear which, being a very localized discontinuity, results in a
much faster micro crack formation, as schematized in Fig. 2.7a. Micro cracks join
to form a macro crack in Stage II of fatigue. Now the crack is already long enough
(>300 μm) to escape shearing stress control and be driven by normal stress which
produces a continuous growth, cycle by cycle, on a plane that is no longer crys-
tallographic, but rather normal to external loads. Ahead of this macro crack two
plastic lobes are generated by stress concentration, as shown in Fig. 2.7b. Even
though these lobes are produced by shearing stresses they are orientated at about
60° with the crack plane, and not 45°. Effectively, LEFM tell us that a surface edge
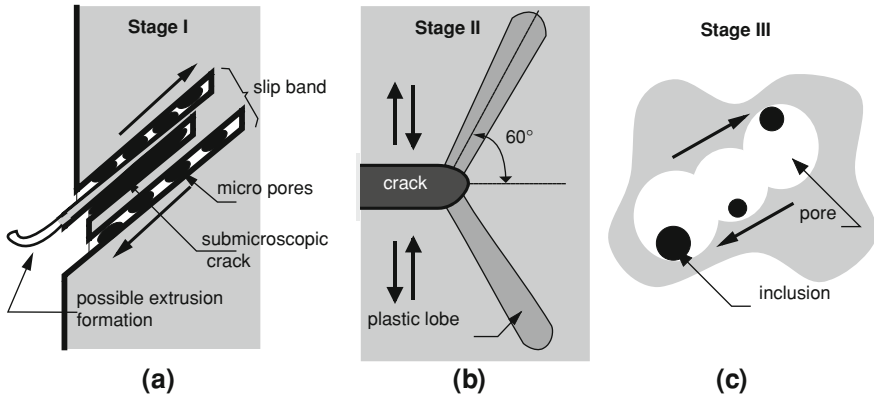crack in a plate in tension generates two lobes the 60° with crack plane. Figure 2.8

Fig. 2.7 Schematic of morphological models of **a** Stage I, **b** Stage II and **c** Stage III of fatigue

[14] shows such crack tip lobes produced under cyclic loads. The sequence starts from compression where the crack is closed, Fig. 2.8a. During successive traction, the crack opens and grows generating the two lobes at the tip, Fig. 2.8b. Next compression recloses the crack. This process leaves some characteristic markings on the fracture surface that will be possible to detect at high resolution in a SEM analysis. These markings are called striations and will be analyzed lather. Finally, Stage III that concludes fatigue growth may happen in two steps. In the first, crack continues to growth by fatigue, but the driving stress field increases continuously because the remaining ligament ahead of the crack decreases. Fatigue, even when it starts as high cycle fatigue, becomes a low cycle fatigue and again shearing stresses become the driving stress, but this time crack growth doesn't proceed on crystallographic planes, but simply in a direction at 45° relative to the maximum stress, as explained in Sect. 1.5.2 (see Fig. 1.67). A schematic of this low cycle crack propagation process was given by Forsyth for aluminum alloys [15] and presented in Fig. 2.9. If there are enough cycles, fatigue, either high cycle or low cycle, terminates with the final failure of the resisting ligament, as shown schematically in Figs. 1.64 and 1.67. It takes just ¼ of cycle, the last, to trigger the collapse of the remaining section. When material behavior is ductile and not brittle, i.e. at least 30 °C above the transition temperature for BCC materials, this final collapse develops through inclusion decohesion from the metal matrix forming cavities or voids, followed by cavities growth, coalescence and fracture, as shown in Fig. 2.10 [16]. In brittle materials final failure occurs by cleavage. From a morphological point of view fatigue crack propagation in Stage II may be transgranular or transcrystalline in high cycle fatigue or intergranular or intercrystalline in low cycle fatigue as shown in Figs. 2.11 and 2.12 [17], respectively. A rather comprehensive map of macroscopic appearance of possible fatigue failures in laboratory test specimens of various shape (cylindrical or prismatic) subjected to a wide range of different loading conditions, stress amplitude with or without stress concentration is offered in Fig. 2.13 [18]. The two characteristic

Fig. 2.8 Crack tip
deformation (lobes) during
loading sequence [14]: **a** after
compression, **b** after
extension, **c** again after
compression
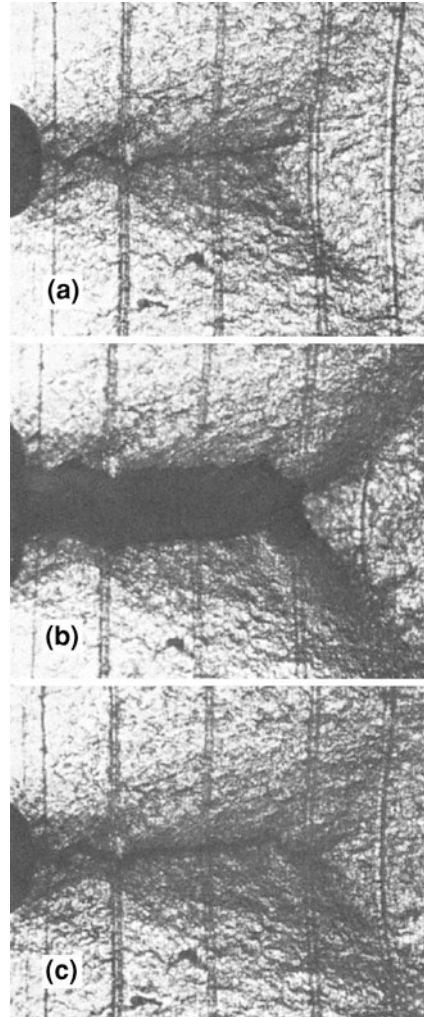
features are the white area within which less or more curved lines develops, also
called beach marks or arrest lines, and the dark one. Beach marks that can be
related in their density and width to the applied stress level and number of cycles
shall not be confused with striations. Beach marks, also called clamshell marks,
are macroscopic morphologic fatigue features that can be seen at naked eye while
striations are microscopic in nature and can be seen only with the aid of scanning
electron microscopy (SEM). Their existence on the fracture surface may have
different origins. As first, the beach marks are produced by changes in crack
growth rates when fatigue is applied in packages of consistent number of cycles.
Each package produces a total crack extension that can be seen without any
enlargement. But beach marks are also produced by other factors than simple

Fig. 2.9 Schematic of low cycle fatigue crack growth [15]. Crack propagation plane is not crystallographic and is inclined relative to the maximum stress
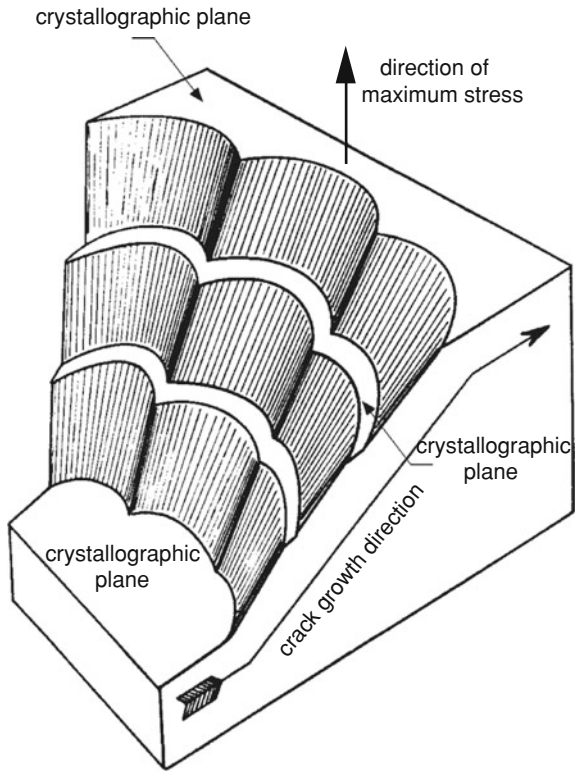
changes in crack growth rates during propagation. The packages of load repetition may have some shorter or longer resting time between each other. The fatigue fractures they generate may exhibit beach marks produced by oxidation of the free surface when the material is idle. Oxidation marks these surfaces differently because of time of exposure and other environmental factors such as air temperature, humidity, pH, etc. and also loads spectra. In facts, many fatigue fractures produced under conditions of uninterrupted crack growth and without load variations do not exhibit beach marks. Therefore, each beach mark denotes a single or more packages of cycles, not a single cycle, and marks progressive stages of crack propagation. At high magnifications, thousands of fatigue striations (microscopic features) can be resolved within each. Sometimes also the direction of stress cycling may have an additional effect on beach marks. This is the case shown in Fig. 2.14 [19]. The rail shown was removed from service when a detail flaw was detected. The rail was subsequently installed in a test facility where it was tested using a train of 75 cars till fatigue failure occurred. The initial flaw is the dark circle from which the beach mark lines evolve as black and with rings departing from the common origin. The reversal in the direction of the test convoy has produced the two different shadings of the beach marks. Back to Fig. 2.13, we observe that beach marks always depart from a single or more initiation points.
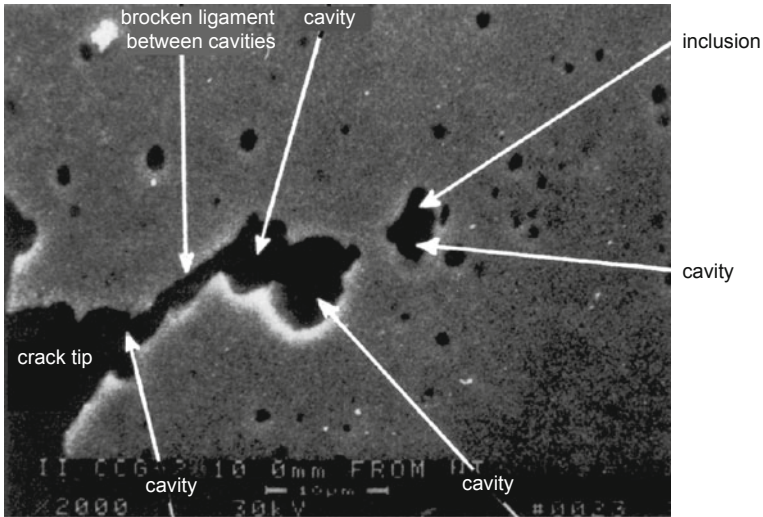
Fig. 2.10 Crack tip cavities formation and coalescence in a ductile fracture process (reproduced with permission of [16])

Generally, under moderate amplitude loads a single initiation site is observed, while high amplitude loads may generate two or more sites. About the dark area that represents the final overload failure, in general when it is equal or even larger than the clear one containing beach marks, as in the first column on the left of Fig. 2.13, it means that cyclic loads had high amplitude therefore after a relatively low number of fatigue cycles the remaining section failed by overload produced by the last 1/4 cycle (Stage III of fatigue). The opposite happens when the load amplitude is low (columns on the right of Fig. 2.13). We may say that low cycle fatigue occurs when the ratio $A_{fatigue}/A_{collapse}$ between the surface interested by fatigue and that collapsed is less than 1. On the contrary, $A_{fatigue}/A_{collapse} > 1$ will be indicative of a long sufferance of the metal under high cycle fatigue that eventually fails. In unidirectional bending the initiation site is located only on one side of the specimen where metal fibers are under traction, while in reverse bending the initiation site may appear on both sides. In rotational bending in which all fibers of the external circumference are equally stressed the initiation site is randomly located choosing the weakest point exactly as in traction. Note how in rotating bending the collapse area contains a darker elliptical feature with one of the two axes lightly inclined relative to fatigue direction. Experience teaches that an angle no lower than 15° is formed in the direction opposite to rotation. The presence of concave beach marks denotes unidirectional bending therefore if they appear on the surface of a specimen tested in tension–tension or tension–compression we shall conclude that the traction was not perfectly axial and some bending occurred. Alike, if concave lines turn into convex beach marks we may conclude that unidirectional bending was not centered. Torsion is worth noting. It produces a brittle fracture along a helicoidally path (last row of the first left
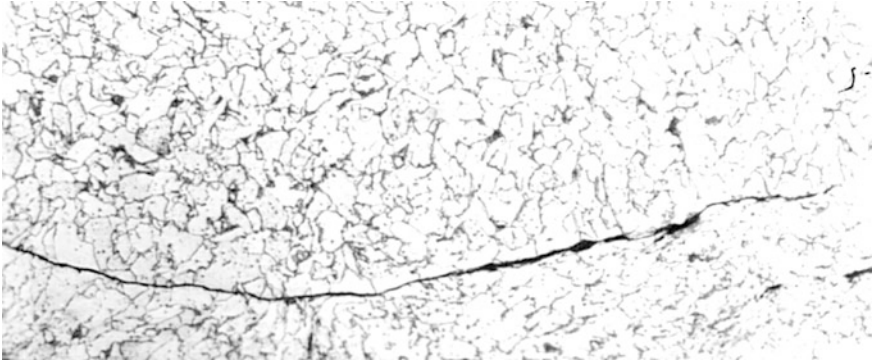
Fig. 2.11 Transgranular appearance of high cycle fatigue observed by Milella in low carbon steel
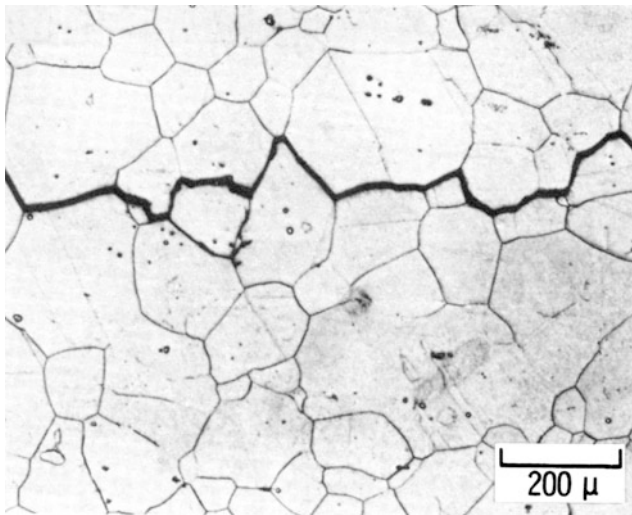

Fig. 2.12 Intergranular appearance of low cycle fatigue in inconel X-750 at 650 °C [17]

column in Fig. 2.13) or a flat failure if the material behaves in a ductile fashion. The difference may be understood analyzing the stress state as in Fig. 2.15. Under pure torsional moment any element free body taken at an arbitrary point on the surface is subjected to pure shearing stress acting on longitudinal and transverse direction, whereas principal stresses acts at 45° being traction on one face of the element and compression on the other, Fig. 2.15a. If principal stresses are high enough and the material is brittle the first macro crack formation will trigger a spiral fracture, Fig. 2.15b sustained by the principal traction stress. Conversely, in case of ductile behavior it may take shearing stress to develop a fracture along a normal plane, Fig. 2.15c, or axial, Fig. 2.15d. In this last case fissures will appear
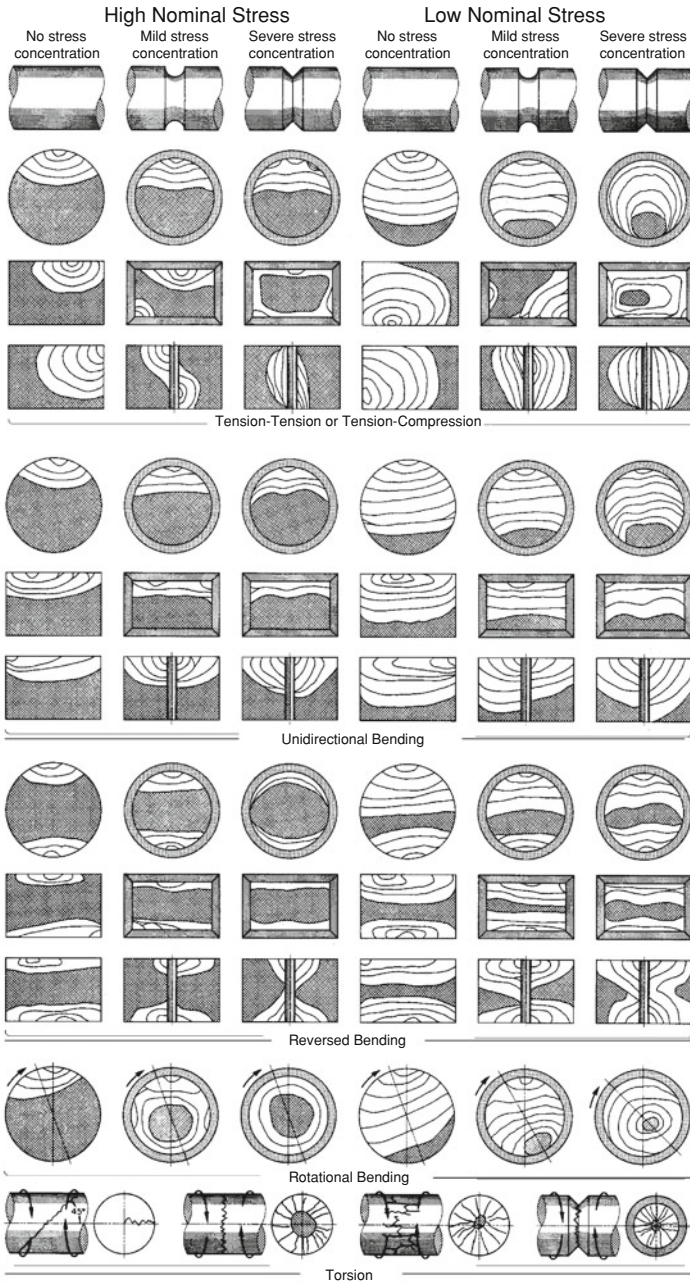
Fig. 2.13 Typical fracture surfaces for laboratory test specimens subjected to a range of different loading conditions [18]

Fig. 2.14 Beach marks in the form of circumferential rings visible at naked eye on the head of a rail failed by fatigue [19]. The initial crack is the dark circle at upper left
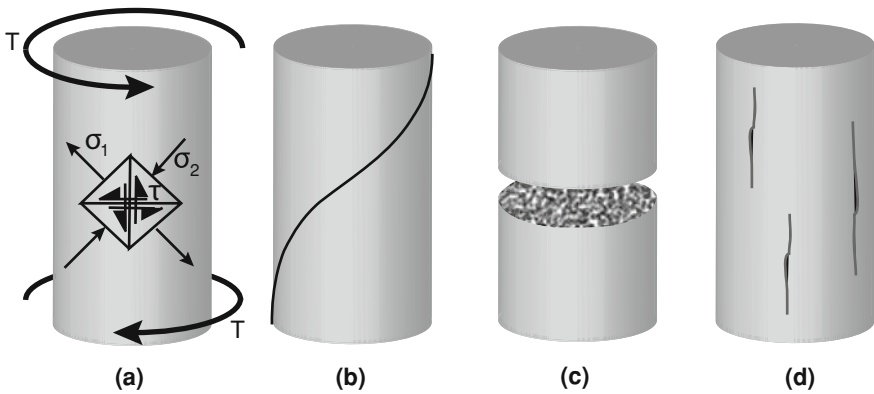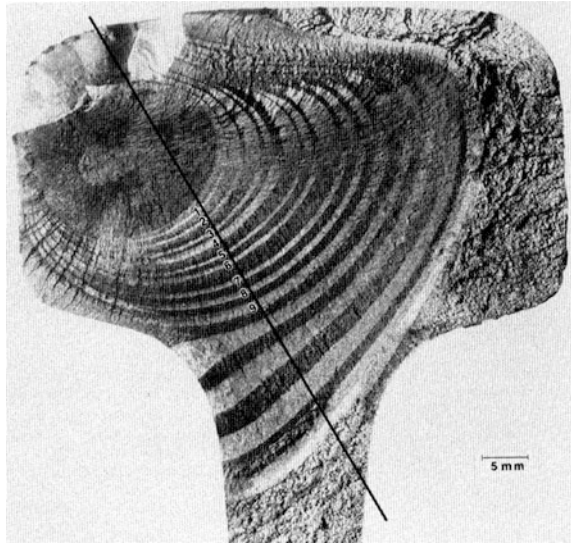

Fig. 2.15 Cylinder in pure torsion. **a** element free body stress state, **b** brittle behavior with helicoidally failure, **c** and **d** ductile failure activated by either longitudinal or transverse shearing stress

on the surface parallel to the axial direction. An example of spiral fracture of a drive shaft of a scooter is shown in Fig. 2.16 [20]. The failure initiated at an inclusion indicated by the arrow. The second type of torsion failure (Fig. 2.15c or last row of Fig. 2.13, second case from the left) is shown in Fig. 2.17 [21]. It refers to an experimental 89 mm ($3\frac{1}{2}$ in.) diameter tractor axle of AISI 1041 steel that had been induction hardened. Note beach marks fanning out from the fatigue crack origin (slightly to left of center, at top). Beyond the beach marks cracking progressed by fast fracture along the hardened perimeter producing two sets of
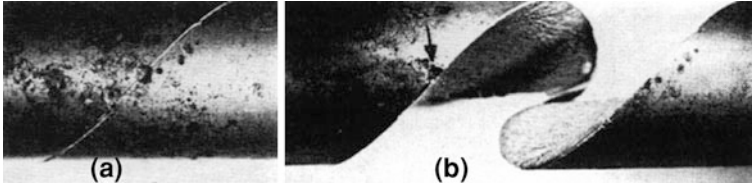
Fig. 2.16 Spiral fracture of a drive shaft of a scooter, starting at surface damage indicated by arrow [20]. **a** mating halves, **b** separated halves

Fig. 2.17 Surface of a bending-plus-torsional-fatigue fracture in an experimental 89 mm ($3\frac{1}{2}$ in.) diameter tractor axle of AISI 1041 steel that had been induction hardened [21]

chevron marks pointing toward the crack origin. The central dark area represents the final fracture by overload.

2.3.1 Real Cases

Following are few examples of real cases of fatigue fracture appearance that may shed some light on the causes that have led to fatigue failure:

1. Fatigue failure in a specimen of 7075-T6 aluminum alloy of rectangular section under unidirectional bending of random amplitude, Fig. 2.18 [22]. Fatigue originated on surface metal fibers in tractions and propagated inside. The ratio $A_{fatigue}/A_{collapse}$ is definitely higher than 1 ($A_{collapse}$ cavers about 40 % of the total area) denouncing a high cycle fatigue with low stress amplitude. Beach marks of different depths are due to crack growth rate variation following random amplitude cycling.

2. Service fracture of 4130 steel shaft with sharp circumferential notch subjected to unidirectional bending fatigue, Fig. 2.19a [22]. Fatigue initiated on the lower part where metal fibers were in traction. Beach marks, due to oxidation when
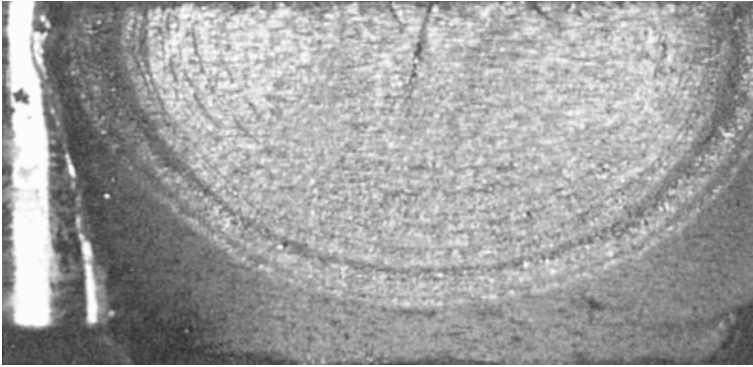
Fig. 2.18 Fatigue failure of a rectangular specimen of 7075-T6 aluminum alloy under unidirectional bending [22]
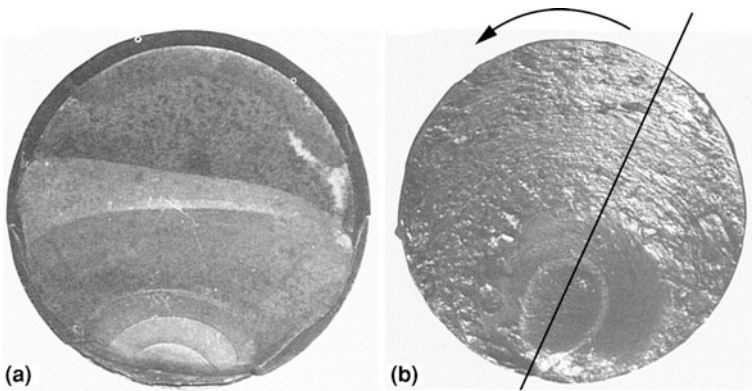

Fig. 2.19   a Unidirectional bending fatigue failure of 4130 steel shaft with sharp circumferential notch [22]. **b** Fatigue failure of 4150 steel shaft subjected to rotating bending [23]

material was idle, are initially concave and become wavy denoting final misalignment in load application. Fatigue has exceeded 50 % of section indicating relatively low amplitude stress.

3. Fatigue failure of 4150 steel shaft subjected to rotating bending, Fig. 2.19b [23]. The section shows beach marks over a large area of the fracture surface. Oval area near the bottom center is the final fracture area. Its major axis is oriented at about 20° relative to the direction of beach marks evolution. This feature indicates that the shaft was rotating in counterclockwise direction. The final area is about 10–15 % of the cross-sectional area which actually suggests low stress amplitude. Fatigue failure initiated at a point of stress concentration. Another example of rotating bending fatigue is that of Fig. 1.4 relative to a journal of an axle rail. Beach marks and the initiation site can be seen.

Fig. 2.20 High temperature fatigue failure under axial loads of a valve stem of 21-2 valve steel [24]. Note the ratchet marks around the circumference that denote the presence of multiple initiation sites (indicated by arrows)
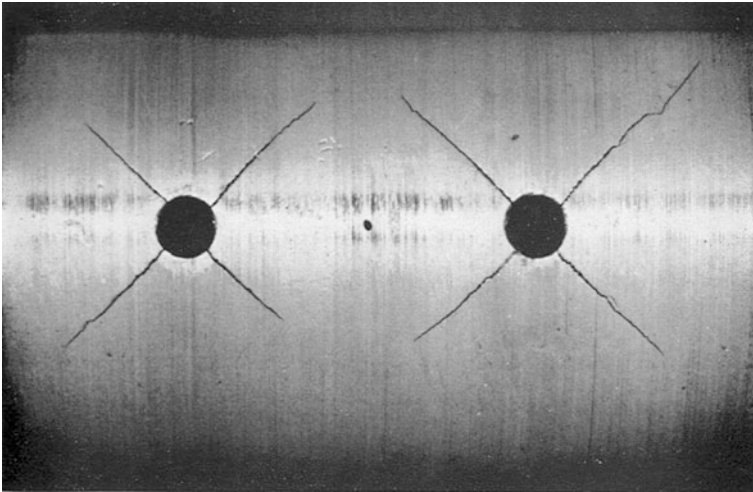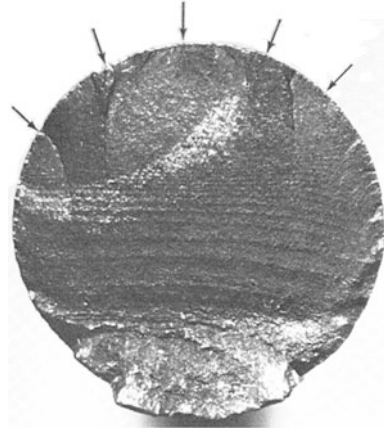

Fig. 2.21 Torsion fatigue failure of an axle of low carbon steel containing two holes [25]

4. High temperature fatigue failure under axial loads of a valve stem of 21-2 valve steel (21 % Cr, 2 % Ni, 8 % Mn, 0.5 % C, 0.3 N) in solution-treated and aged condition and faced with stellite 12 alloy (30 % Cr, 8 % V, 1.35 % C, rem Co), Fig. 2.20 [24]. Note the ratchet marks around the circumference that denote the presence of multiple initiation sites (indicated by arrows). The wavy shape of beach marks is indicative of off-axis load that has introduced a bending component.

5. Torsion fatigue failure of an axle of low carbon steel containing two holes, Fig. 2.21 [25]. Fatigue cracks initiated from holes that represent points of stress concentration. To feed the cracks has been traction principal stress acting on a plane at 45° to the axis (see Fig. 2.15a). The presence of two cracks at right

Fig. 2.22 Failure by
torsional vibrations in an oil
engine crankshaft [25]
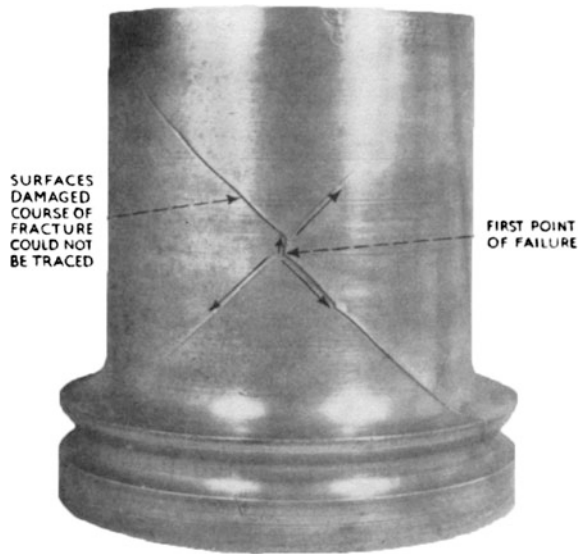
angles to each other making an X suggests that the torque has been of a
reversing character. Since the cracks are of approximately the same extent the
indications are that the torque reversals have been of equal magnitude. This
applies, however, only so long as the cracks are in a comparatively early stage
of development, as beyond this stage one crack usually takes the lead and such
inferences are no longer justified.

6. Failure by torsional vibrations in an oil engine crankshaft, Fig. 2.22 [25]. Ini-
   tiation started at the journal nearest the flywheel from a longitudinal inclusion
   afterwards cracks propagated along two X directions as in the previous case.
   Reversed bending failure in 1046 steel with a hardness of approximately HRC
   30, Fig. 2.23 [26]. Rubbing has obliterated the early stages of fatigue cracking,
   but ratchet marks are present to indicate locations of crack initiation on both
   sides of the central region failed by overload that appear rougher than the
   fatigue areas.

7. Fracture surface of the piston rod of a pneumatic hammer, Fig. 2.24 [26]. It may
   seem a rotating bending failure because of the lateral center oval area denoting
   final fracture (see case 3 marks and Fig. 1.96b), but it is not. The cracks were
   caused by tensile stresses developed due to non-axial loading, which were
   probably supplemented by compressive stress waves that became tensile when
   reflected. The small radial ridges near the periphery show that a series of cracks
   broke out there and joined together to form several crack fronts separated by the
   large ridges; ultimately, the crack fronts merged into a single annular one sur-
   rounding the zone of final failure.

Fig. 2.23 Reversed bending failure in 1046 steel [27]. Rubbing has obliterated the early stages of fatigue cracking. Ratchet marks along circumference indicate locations of crack initiation

Fig. 2.24 Fracture surface of the piston rod of a pneumatic hammer failed under tension–compression loads [27]. The small radial ridges near the periphery show initiation sites that form several crack fronts that merged into a single annular one
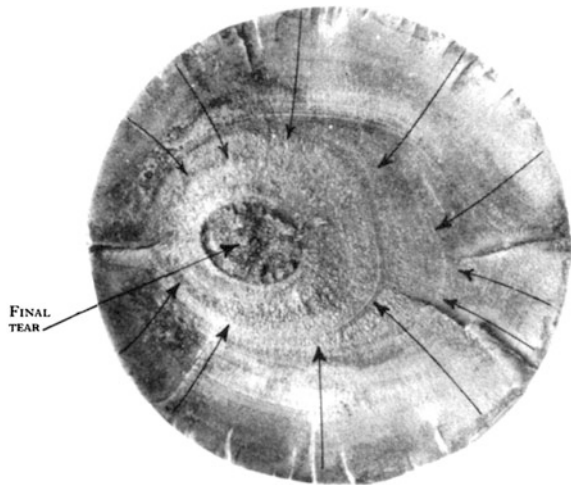
2.4 Origin of Fatigue Striations

In the last paragraph we have been showing how beach marks evidence packages of cycles. Now we will discuss of any single cycles that may leave a mark on fatigue fracture surface. At variance with beach marks that can be seen at naked

Fig. 2.25 Crack tip blunting and growth in during loading and closure upon unloading that leads to striation formation through the crack tip plastic slip mechanism [30]
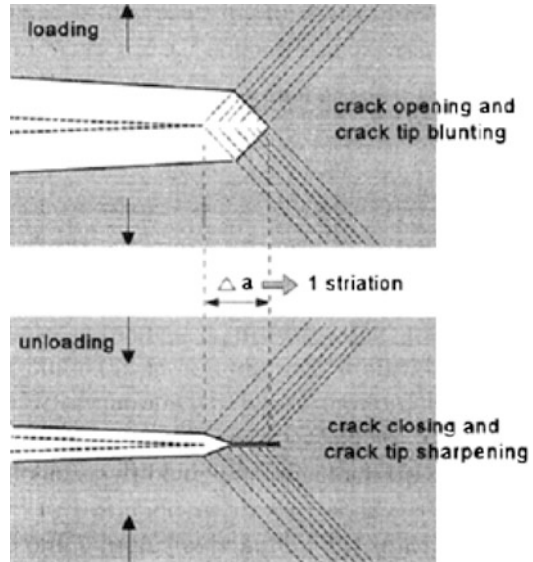
eye, the trace of a single cycle can be seen only at high magnification, like in optical or better SEM or TEM analysis. This trace was originally called slip band by Thompson e Wadsworth [28] and later striations by Nine e Kuhlmann-Wilsdorf [29]. Striation is the most striking fine scale feature left on the fatigue surface, a kind of microscopic fingerprint that identify fatigue crack growth. The reference basic model in striations generation is that of crack tip plastic slip schematically shown in Fig. 2.25 [30]. During loading phase the crack is opened by normal stress that activates plastic slips at the tip. Fracture mechanics is predicting that this flow happens along two symmetrical directions (see Figs. 2.7b and 2.8). In this phase crack tip blunts and grows by material decohesion associated to dislocations flowing into the tip or generated by stress concentration. This type of plastic deformation is not completely recoverable. Therefore, upon unloading the blunting is squished, but a new free surface remains head of the former crack with a new sharp tip. The irreversible process has made the crack grow by a quantity Δa. It is this step by step process of blunting and re-sharpening at each cycle that leaves on the crack path a kind of footprint that we call striation, as schematized in Fig. 2.25.

Laird has given a rather different interpretation of striation formation based on the so called plastic relaxation of crack tip that is schematized in Fig. 2.26 [31]. Figure 2.26a refers to initial condition where crack is idling. Then the load is applied, Fig. 2.26b and crack tip plastic slips occur on both sides. At maximum load, Fig. 2.26c, the tip is fully blunted. With load inversion, Fig. 2.26d, crack tip closure takes place by reverse plastic flow that leaves the crack in the same initial condition, but with a new formed elementary free surface that testifies the crack growth, Fig. 2.26e. Last stage, Fig. 2.26f, represents the new loading phase similar to (b). Note that the process, that Laird called plastic relaxation, is based on the
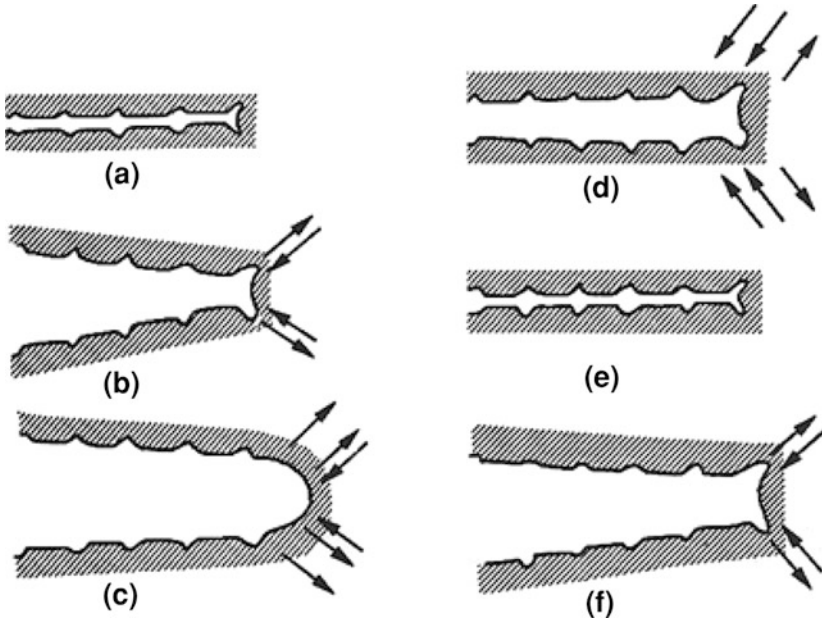
Fig. 2.26 Schematic of striations formation based on crack tip plastic relaxation [31]

hypothesis of plastic collapse of crack tip during the unloading and closure phase that leads to tip concavity. Some characteristic profiles associated with crack propagation in Stage II of fatigue and to the above mechanism of fatigue formation are shown in Fig. 2.27 [31]. The first, Fig. 2.27a, indicates a fatigue propagation under relatively high stress amplitude, yet lower than yield strength. It consists of mating concave-convex parallel profiles on the two opposite fracture surfaces. Type (b) is characterized by the presence of small lateral cracks, indicated by arrows, and is characteristic of brittle striation, which will be discussed later. Types (c) and (d) are similar to type (a), but the smaller dimension of depressions indicates lower stress amplitudes. Types (a), (c) and (d) striation are called ductile striation since they are based on one of those mechanisms just seen that are based on crack tip plastic slip.

2.4.1 Striation Observation

An example of ductile striations of the type presented in Fig. 2.27a, c and d is shown in Fig. 2.28a [15]. They were observed by Forsyth on 7,5 Zn-2,5 Mg aluminum alloy. The brittle case of Fig. 2.27b is shown in Fig. 2.28b and c [15]. The material is always 7,5 Zn-2,5 Mg aluminum alloy. In this case the micro cracks emanating from each propagation step can be seen. Figure 1.106c shows

Fig. 2.27 Possible crack propagation profiles according to Laird's model of striations formation [31]
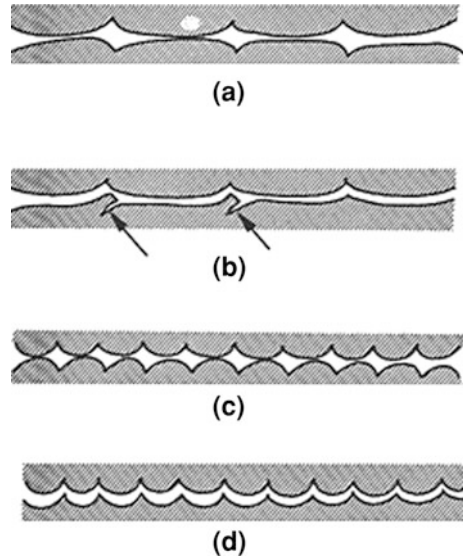
the plastic enclaves or lobes (see Figs. 2.7b and 2.8), that appears on a free surface as tiny flakes, associated with the growth of brittle striations. The width so far measured of striations varies from a minimum of about 0.1 μm to a maximum of about 2.5 mm. It has been found [32] that in the transition between Stage I and Stage II of fatigue, when micro cracks turn into macro cracks that can be opened by normal stresses (the so called fatigue threshold), striations width is some order of magnitude higher than the real crack propagation rate and keeps constant at about 0.1 μm (see Fig. 2.29 and Sect. 10.6). It is likely to happen that in this threshold region a single striation can be formed only after thousands of cycles.

Grinberg has been the first to recognize that the minimum striation size was in the order of a tenth of a micron, from one to three orders of magnitude higher than the real growth per cycle, as shown in Fig. 2.29 for an annealed iron in humid air [33, 34]. This has been recognized in Aluminum and its alloys, magnesium, nickel, titanium alloys and many steels. Figure 2.30 shows striations observed by Milella on carbon steel type Fe 510 in the threshold zone. Striation width is about 0.1–0.2 μm, but the real growth rate should be 10^{-4}–10^{-3} μm/cycle, i.e. from one thousand to one hundred folds lower. On a microscopic scale fatigue crack propagation evolves on different planes. This is due to metallurgical reasons and, in particular, to the fact that fatigue crack propagates along grains that are not necessarily coplanar, as schematized in Fig. 2.31 [35]. Striation are grouped in areas of homogenous propagation separated by tear ridges in which material fails by shearing resulting in the apparent continuity of the fatigue advancing front. The areas of homogenous propagation represent single grain. The various propagation areas may join as, for example, 7 and 8, in Fig. 2.31, that merge into 9 or separate as 4 that bifurcates into 5 and 6. In each of these individual areas the crack propagation direction, indicated by arrows, may not be exactly the same.
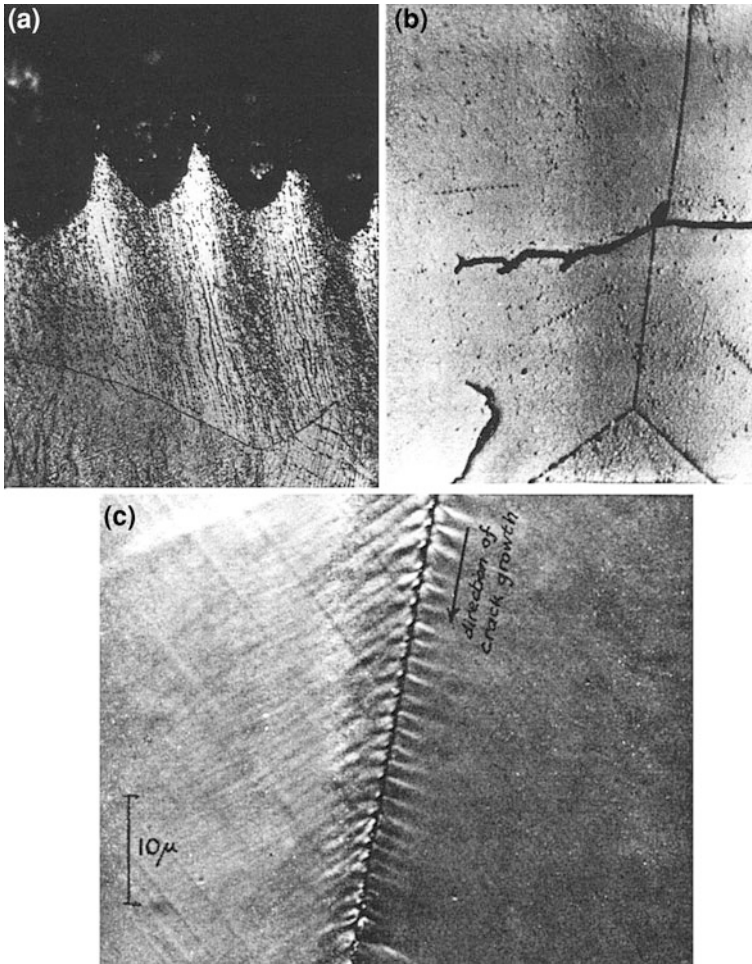
Fig. 2.28 **a** Ductile. **b** brittle striations observed by Forsyth on 7.5 % Zn–2.5 % Mg aluminum alloy [15]. **c** plastic enclaves observed on a free surface associated with brittle striations [15]

Striations are always bowed out in the direction of crack propagation because their growth evolves more easily at center than on borders where they are blocked by grain boundaries and other barriers. Some areas of local propagation, as 7 and 13 in Fig. 2.31, are convex others, as 8 and 12, are concave on one side and the opposite on the other side thus forming the concave-convex mating surfaces and profile as shown in Fig. 2.31. It is rather common to observe areas of homogenous propagation separated by others that do not show any signs of fatigue, specifically striations. An example is shown in Fig. 2.32 for a 6Al−4 V titanium alloy [35]. It may also happen that during crack propagations the two mating surfaces slightly move relative to each other. This causes the loss of perfect mating between elevations and valleys that may results in a continuous hammering between pikes

Fig. 2.29 Fatigue crack growth rate (*circles* and *line*) versus stress intensity factor ΔK in annealed iron in humid air. Also shown are the striations width measurements [32, 33]
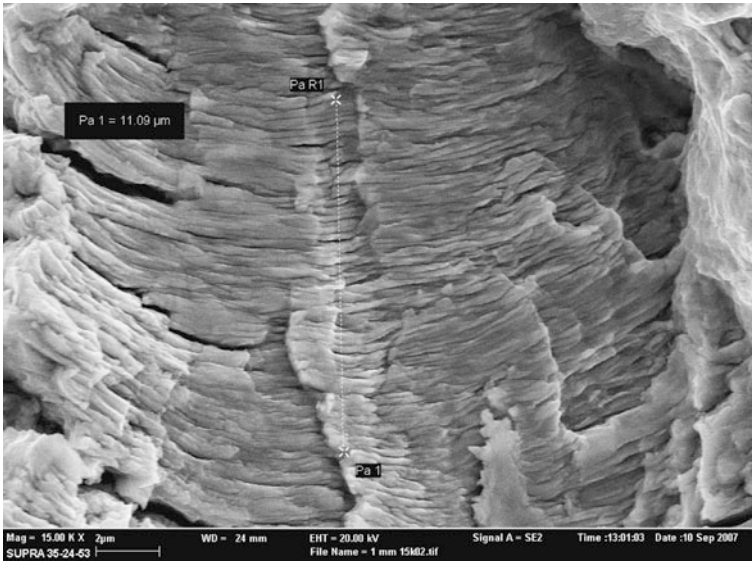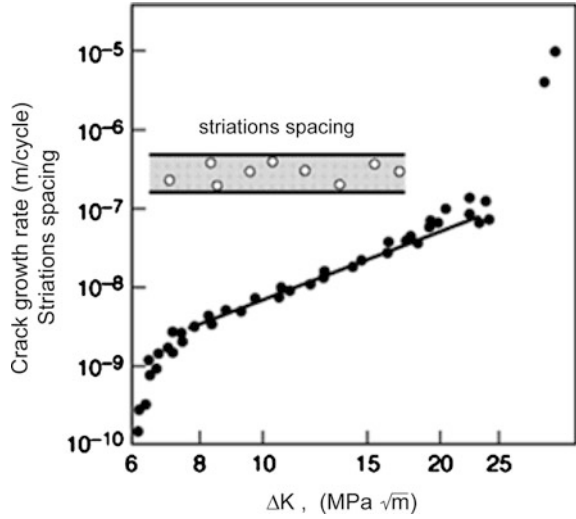

Fig. 2.30 Striations observed by Milella on Fe510 carbon steel in the fatigue threshold zone. Striations width is about 0.1–0.2 μm, but the real growth rate is significantly lower, about two orders of magnitude

during the unloading phase. These signs, less or more marked depending on the relative surfaces offset, are called tire tracks. An example of tire tracks is shown in Fig. 2.33 for 2024-T3 aluminum alloy [35]. Another cause for tire tracks formation is the presence of hard particles that hammer opposite face, always due to surfaces
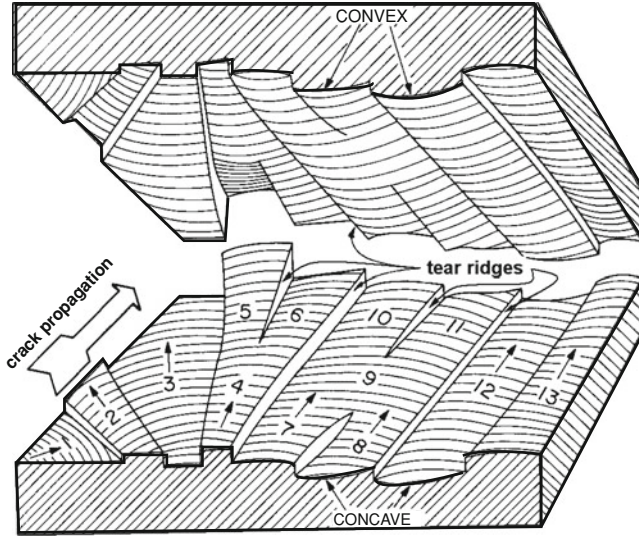
Fig. 2.31 Schematic of striation growth in grains and their merging or separation (reproduced with permission of [35])
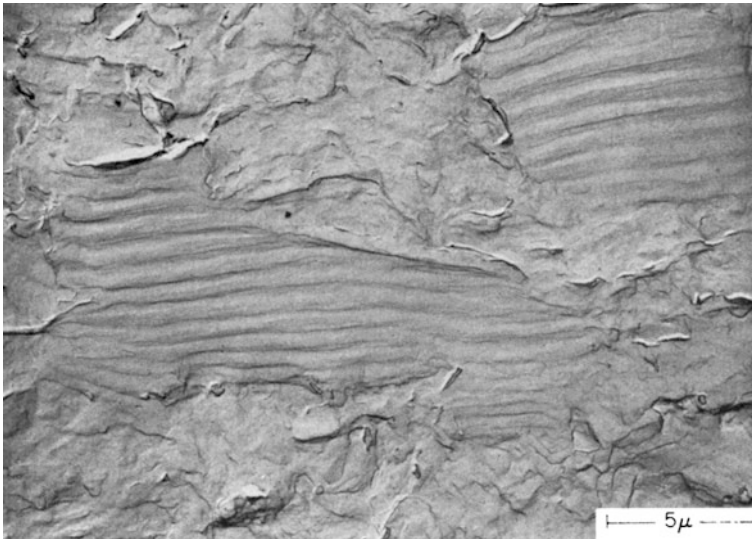

Fig. 2.32 Fatigue striations in 6Al-4 V titanium alloy [35]. Same area shows striations formation other doesn't

offset. This is shown in Fig. 2.34 [35]. Quite often it may happen to see cracks between striations, as in Fig. 2.35.

   These cracks develop after the main crack has passed and are due to local stress states. Sometimes they open on a plane perpendicular to that of propagation.
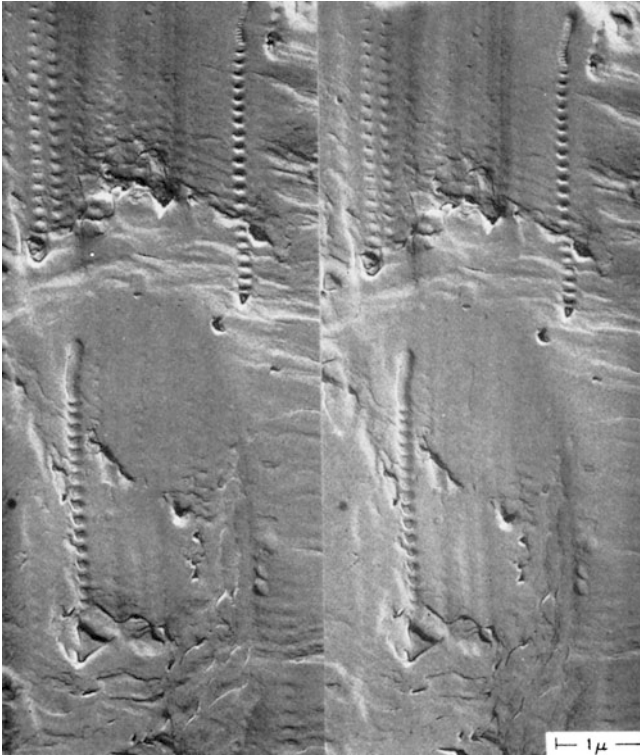
Fig. 2.33 TEM of 2024-T3 aluminum alloy showing characteristic tire tracks signs due to surface hammering [35]. Pair stereo replica

Another characteristic feature that may be observed on each single striation, as in Fig. 2.35, is the presence of smaller closely spaced striations. The origin of these closely spaced striations may be explained by the striation mechanism proposed by Gross and schematized in Fig. 2.36. In this mechanism, basically similar to that of Fig. 2.25 and based on two stages process of blunting and closure re-sharpening of the crack tip, compressive closure stress, Fig. 2.36b, may activate a series of slip lines ahead of the crack tip that leave a trace on the main striation.

2.4.2 Ductile and Brittle Striations

Forsyth [14] recognized and described two general types of striations: the ductile and the brittle one. They are schematized in Fig. 2.37 [36]. Both types of striations are transgranular. Ductile striations lay on different individual planes corresponding to single grains that macroscopically form, all together, a plateau normal to the maximum tensile stress direction, as shown in Fig. 2.37a. They are called
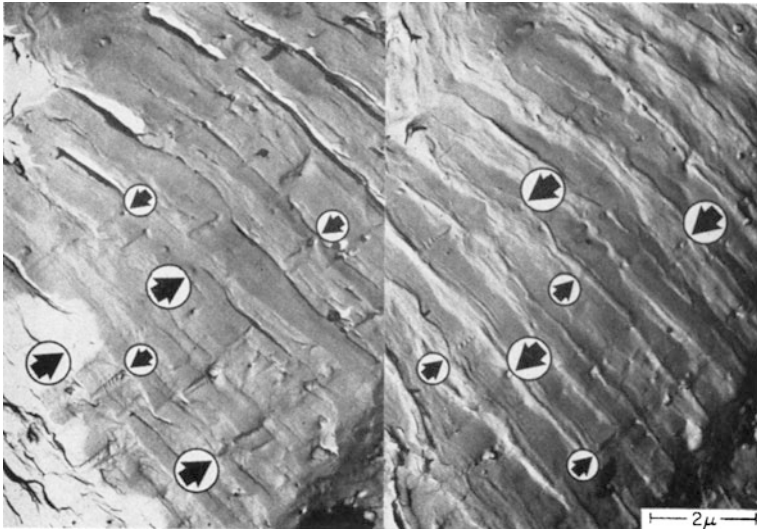
Fig. 2.34 TEM of 2024-T3 aluminum alloy showing characteristic tire tracks signs due to hammering operated by hard particles indicated by arrows on offset opposite surface (reproduced with permission of [35]). Pair stereo replica

Fig. 2.35 Cracks between striations observed by Milella produced after the crack has passed

ductile because the material ahead of crack tip undergoes plastic deformations that produce the typical curved arrays by which they advance on the fracture surface. Brittle striations, instead, develop always on crystallographic planes, usually (100)
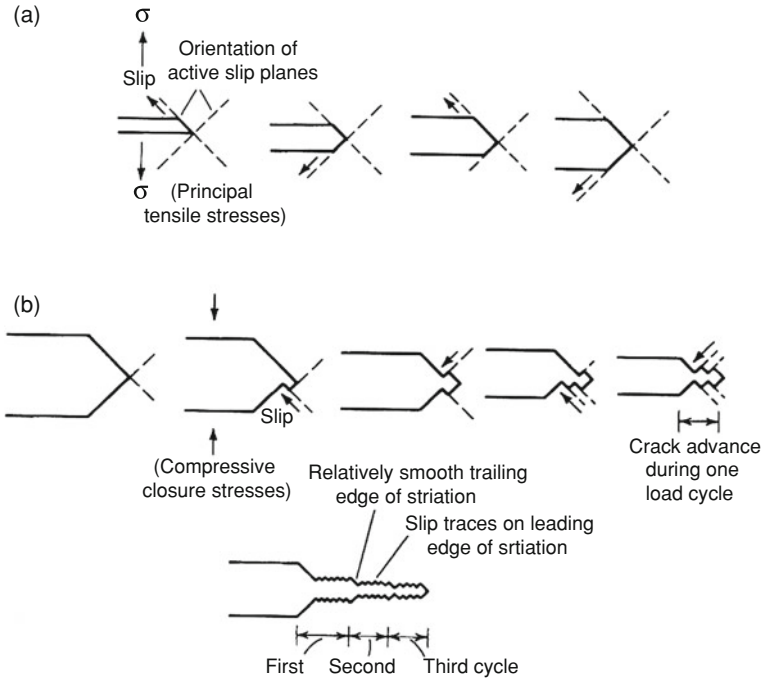
Fig. 2.36 Schematic mechanism of fatigue crack propagation by alternate slip at crack tip: **a** crack opening and crack tip blunting by slip. **b** crack closure and crack tip re-sharpening by partial slip reversal (reproduced with permission of [36]). Reprinted with permission of ASM international.

planes [38], and appear as concentric circles departing from the initiation site, quite often brittle inclusions, Fig. 2.37b. This gives brittle striations the typical flat appearance with any apparent (macroscopic) plastic deformation. Brittle striations are always associated with corrosion assisted fatigue and, in particular, with hydrogen absorption, as it will be discussed in Sect. 16.4. Example of ductile and brittle striations are shown in Fig. 2.38 [39, 40] on 7.5 Zn–2.5 Mg, 7178 and 2014 aluminum alloys.

A characteristic feature of brittle striations is the uniform, flat and woody year-ring propagation surface that doesn't propagate in single crystals but on crystallographic planes that are cleavage planes. On these planes a continuous radial array of tiny cleavage steps appears that develops transverse to the circles that represent single propagation events that point back to fatigue fracture origin, Fig. 2.37b and d. Originally observed by Forsyth on aluminum alloys, brittle striations have been found also on nickel, carbon and stainless steels. Figure 2.39 [41] is another example of brittle striations on admiralty alloy operating in a water solution of ammonia that provided the corrosion environment and, in particular, hydrogen. Four concentrically circles appear with the array of continuous cleavage steps.
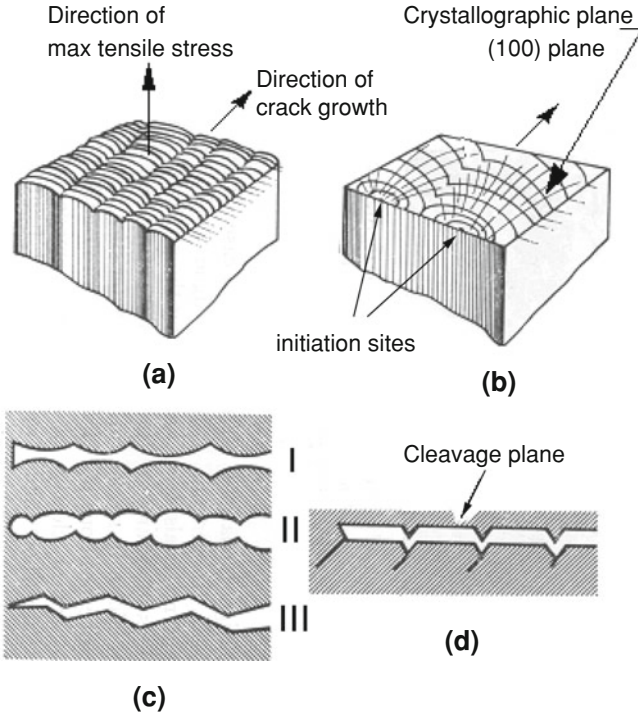
Fig. 2.37 Schematic difference between ductile and brittle striations: **a** ductile striations. **b** brittle striations. **c** ductile profiles. **d** brittle profiles (modified from [37])

Under conditions of corrosion fatigue the crack tip doesn't open and blunt as shown in Fig. 2.26c or 2.36, but remains sharp. This allows the formation of an elastic stress field of high amplitude and triaxiality ahead of the crack tip that favors hydrogen adsorption, Fig. 2.40a. Hydrogen embrittles the metal through different mechanisms that will be discussed in Sect. 14.4. The high elastic stress field in a material become brittle breaks the metal ahead of the crack tip along a crystallographic plane or cleavage plane, Fig. 2.40b. Note that brittle striations are difficult to detect just because the crack tip doesn't open, which is typical of brittle fracture, and any sign of plastic deformations (ductile striations) is left on the fatigue fracture surface. Striations of Fig. 2.39 are visible because every four to five cycles a light overload was applied just to open crack tip and mark the growth. The circles visible in Fig. 2.39 are precisely those overloads marks. An interesting example of fatigue propagation under hydrogen embrittling conditions is offered in Fig. 2.41 [42]. The fatigue cycling in dry air has produced the characteristic ductile striations, Fig. 2.41a. Same steel, but in a hydrogen gas environment has completely changed its behavior developing brittle striations, Fig. 2.41b. Very often, hydrogen produces a characteristic grain boundary embrittlement, described in Sect. 14.4.3, which results in an intergranular separation of crystals. This
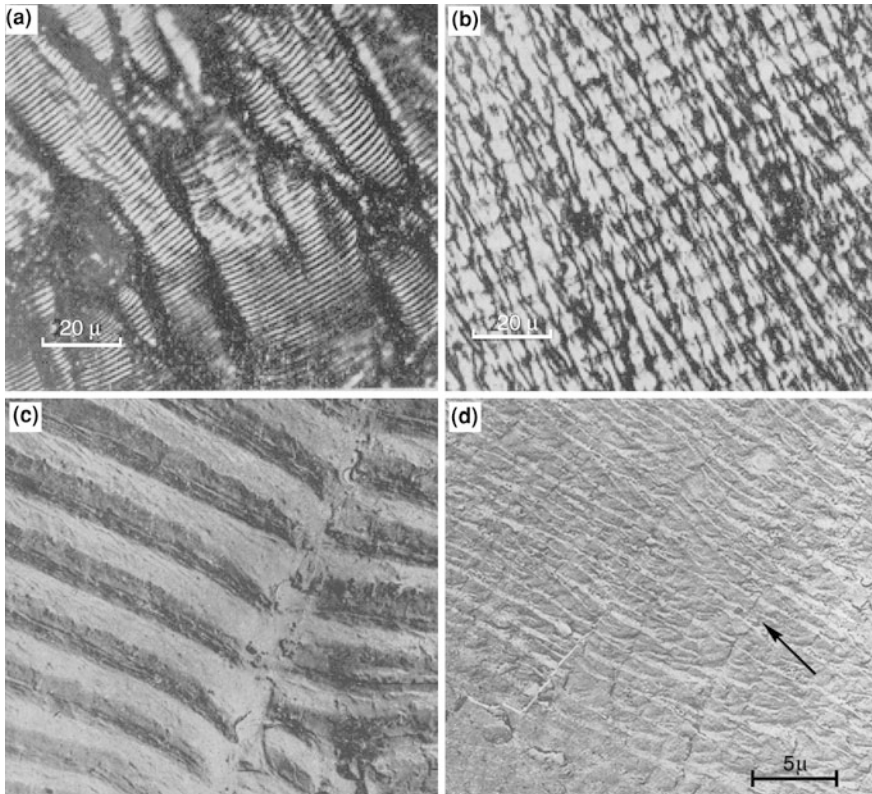
Fig. 2.38 **a** Ductile striations, **b** brittle striations on 7.5 Zn–2.5 Mg aluminum alloy, **c** ductile striations on 7178, **d** brittle striations on 2014 aluminum alloys [39, 40]. **a** and **c** observed with optical microscopy, **c** and **d** with TEM. *Note* in **b** the array of groves transverse to striations circles better identify in **d** as cleavage steps

morphology of fatigue failure is so typical that any time an intergranular separation appears the first hypothesis made is always that of hydrogen embrittlement and in most cases it's the wright one. Figure 2.42 is an example of this kind of fatigue failure observed by Milella on a 1,100 MPa NiCr high strength gear steel, hardened to HRC 55 that failed after 1,000,000 cycles with $R = 0$.

2.4.3 Striations and Fatigue Cycles

The question of whether or not a single striation would correspond to a single fatigue cycle was first answered by Forsyth e Ryder [43] who used programmed constant amplitude fatigue cycles spaced by overload marking cycles. On the fracture surface it was possible to pick up these overload markers that were

Fig. 2.39 Transgranular brittle striations by corrosion fatigue on admiralty alloy in water diluted ammonia (reproduced with permission of [41]). Four concentrically circles appear intersecting the continuous array of cleavage steps. Black arrows indicate propagation direction
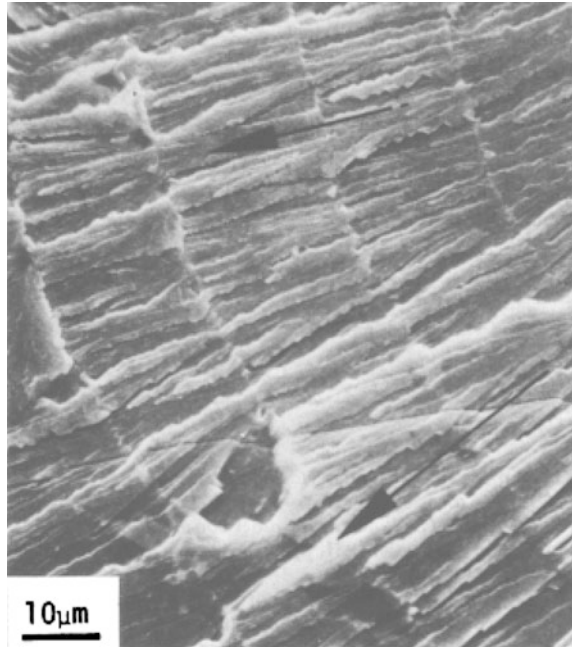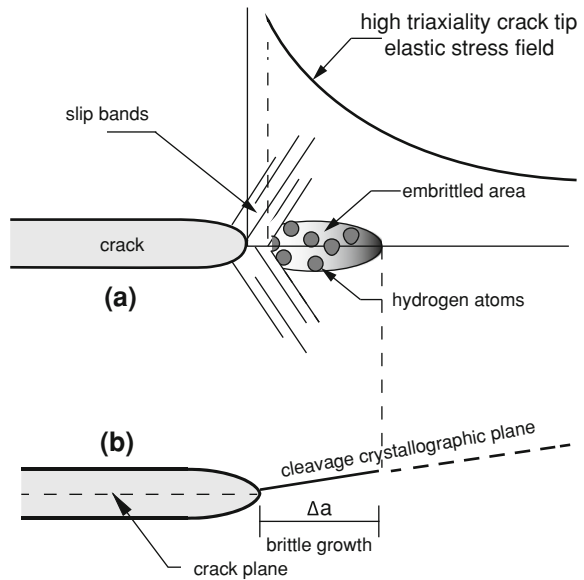

Fig. 2.40 Schematic of crack tip brittle growth by corrosion fatigue that leads to brittle striations formation: **a** hydrogen absorption driven by high triaxiality elastic stress field, **b** brittle growth

separating the constant amplitude cycles and count these last. In this manner it was verified that indeed there was a correspondence between cycles and striations in that there were as many striations as the cycles imposed to the specimen
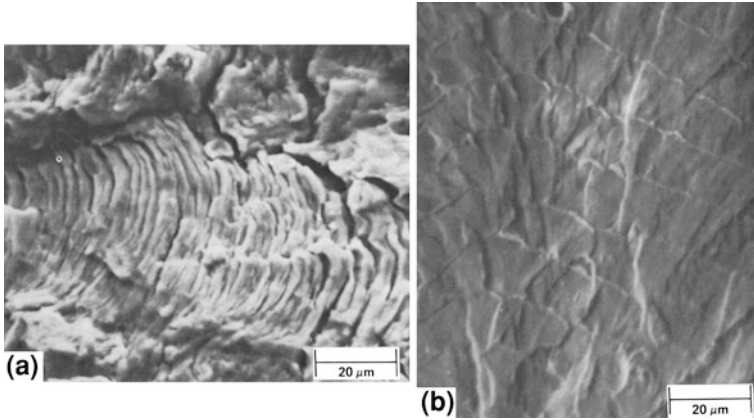
Fig. 2.41 **a** Ductile striations and **b** brittle striations developed in a ferritic low strength steel stressed **a** in dry air and **b** in hydrogen gas environment [42]
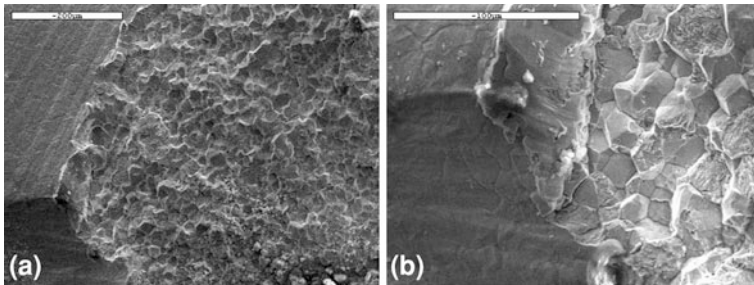

Fig. 2.42 **a** SEM morphology of intergranular fatigue failure of a gear tooth of NiCr steel hardened to HRC 55 observed by Milella. **b** detail of the initiation site

and each striation had a width proportional to the corresponding cycle amplitude. An example of such a technique of programmed load fractography used by Pelloux et al. on 2124–T351 aluminum specimens is shown in Fig. 2.43 [44]. The loading sequence A, B and C programmed in number and amplitude of cycles is repeated after an overload of two or four cycles. Each block of cycles is clearly detectable by SEM fractography analysis. The two and four overload markers can be identified on the fracture surface.

The number of cycles applied in each block is equal to those counted on the fracture surface. The different striations amplitude is also evident and is proportional to cycle amplitude. Moving from high cycle fatigue to low cycle fatigue regime, striations gradually disappear giving place to fractographic signs similar to those that characterize ductile fracture, according to what has been said about Stage III of fatigue in § 1.7. A clear example is shown in Fig. 2.44 [45] for 6061-T651aluminum alloy. Figure 2.44a refers to Stage I damage nucleation phase almost featureless at low magnification. Figure 2.44b shows the region of crack

Fig. 2.43 Programmed loading fractography to evidence packages of fatigue cycles in 2124-T351 aluminum alloy [44]. Loading sequence *A*, *B* and *C* are repeated after being separated by overloads *D*. The number of cycles given in each block can be verified on the fracture surface by SEM analysis
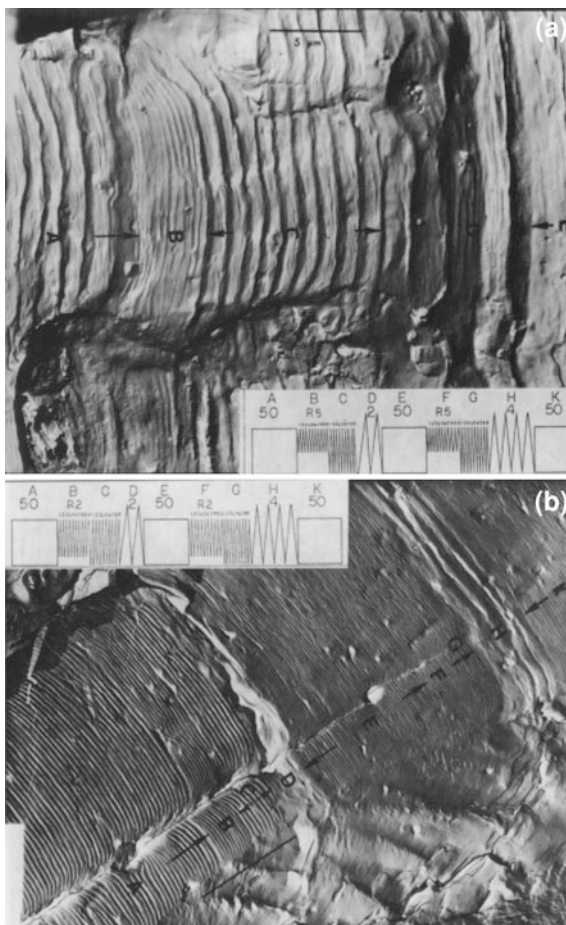
propagation without striations, but with intergranular cracks and voids formed around inclusions. Intergranular separation is typical of low cycle fatigue, as said in Sect. 1.4.2. Fatigue striations disappear also in high cycle fatigue during the early phase of macroscopic crack propagation at very low amplitudes close to the threshold stress intensity factor ΔKth (see Figs. 10.22 and 10.23). Even though striations are characteristic of high cycle fatigue their observation on the fatigue fracture surface may not be so simple. This is the case of high strength materials having low deformation at fracture. These precipitation hardened metals are characterized by very small grains, 10–15 μm. They offer a thick grid of hard barriers to dislocations motion that are not allowed to extend and become so long to develop continuous arrays of ductile striations.

Albeit fatigue striations are due to a plastic flow that opens and blunts crack tip, an important role in their visibility, at least with the aid of the electron microscope, is played by corrosion or, at least, oxidation. It has long been recognized that
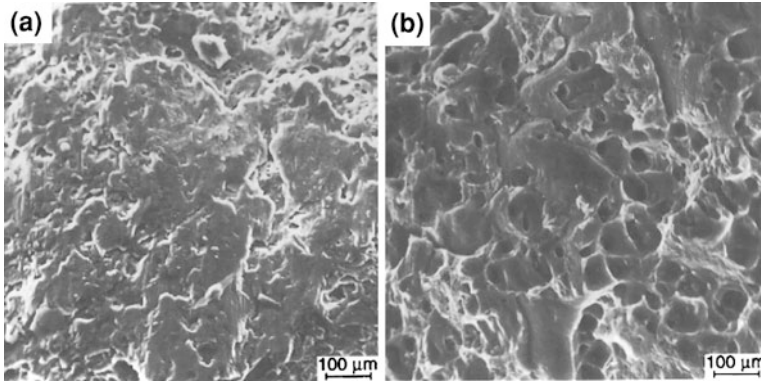
Fig. 2.44 SEM analysis of the fracture surface of 6061-T651 aluminum alloy failed by low cycle fatigue showing: **a** featureless crack initiation region, **b** voids and intergranular cracks (reproduced with permission of [45])

Fig. 2.45 SEM examination of the fracture surface of a waspaloy specimen fatigued at 500 °C **a** in vacuum and **b** after resting in air (Milella). Striations in vacuum are barely observed
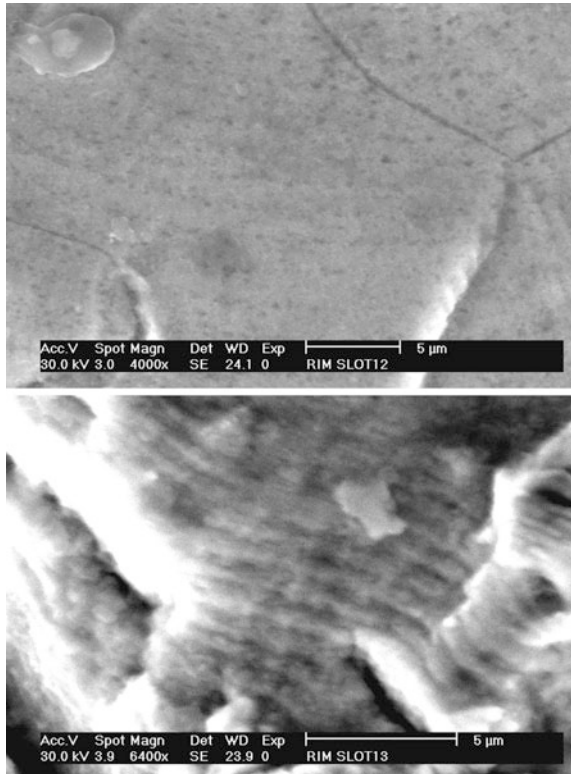
fatigue in vacuum leaves very light signs of striations when it doesn't leave any at all. Figure 2.45 is an example of scanning electron microscope observations by Milella of fatigue striations on waspaloy at 500 °C in vacuum and air, respectively.

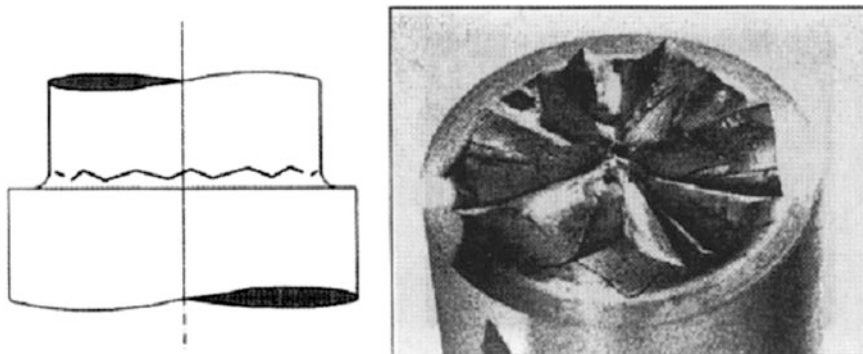**Fig. 2.46** Fatigue failure obtained under cyclic torsion in round carbon steel specimen (0.45 % C) with a fillet notch [50]. Note the characteristic factory roof type fracture surface

Fatigue tests were initially run in vacuum where striations are barely visible inside grains, Fig. 2.45a. Tests were interrupted to check specimens and then started again under vacuum. During these resting periods air was allowed to enter into the environmental chamber. The lesson learned from experience is that in such cases tests at restart show all signs of fatigue in air, growth rate included, even though they are run in high vacuum. This can be seen in Fig. 2.45b where striations appear after air has been admitted in the test chamber and test restarted, though in high vacuum. Striations spacing in vacuum seems to be larger than in air when it is well known that fatigue in vacuo cannot be more dangerous than in air.

This apparent incongruence may be explained by saying that in vacuum each striation doesn't correspond to a single fatigue cycle since several cycles are needed to produce a single striation. Same result has been obtained on Ti-6Al-4 V [46, 47] by Pelloux and by Wadsworth and Hutchings on aluminum, copper and gold. They found that the ratio between life in air and under high vacuum (10^{-5} mm Hg $\sim 1.4 \cdot 10^{-4}$ atm) was about 1:20 for copper, 1:5 for aluminum and 1:1 for gold. This last result is particularly indicative since gold is very resistant not only to corrosion but also to simple oxidation. This actually confirms that in striations formation an environmental effect, namely surface oxidation, must take a role. It has been argued that in vacuum during the unloading phase and, in particular, during the load inversion a more or less complete re-fusion or healing of the sliding facets can take place because oxidation has not occurred. This delay when not stops at all the fatigue process. This is particularly true under very low amplitude stress when plastic slips are very limited and irreversible damage is very low. McClintoc and Pelloux [48] proposed a striation formation mechanism based on a surface oxidation process. Finally, it is useful to remember that no striation will appear if the crack is opened by a cyclic torque. Shearing stress does not produce striations. An example of macroscopic appearance of a carbon steel specimen broken under cyclic torque is presented in Fig. 2.46 [49].

The appearance is that of factory roof type. If one of those roofs were observed no sign at all of striations would appear at SEM analysis.

References

1. Neumann, P.: Bildung und Ausbreitung von Rissen bei der Wechselverformung. Zaitschrift f. Metallkunde H **11**, 780–789 (1967)
2. Forsyth, P.J.E.: International Conference on Fatigue. Inst. Mech. Eng. (1956)
3. Forsyth, P.J.E., Stubbington, C.A.:The Slip band extrusion effect observed in some aluminum alloys subjected to cyclic stress. Nature. vol. 175, p. 767 (1955)
4. Forsyth, P.J.E.: Some observations on the nature of fatigue damage. Phil. Mag. vol. 2, p. 437, (1957)
5. Forsyth, P.J.E.: Proceedings of Royal Society A242, 198 (1957)
6. Forsyth, P.J.E., Stubbington, C.A.: Slip band extension effect observed on copper. J Inst Metals. **86**, 90 (1957–1958)
7. Klesnil, M., Lukáš, P.J.: Iron and Steel Institute. **203**, 1043 (1965)
8. Cina, B.J.: Iron and Steel Institute. **194**, 324 (1960)
9. Cottrell, A.H., Hull, D.: Extrusions and intrusions by cyclic slip in copper. Proc. Roy. Soc. **A242**, 211–213 (1957)
10. Kocanda, S.: Fatigue Failure of Metals. Sijthoff & Noordhoff Int Pubs, Alphena/d Rijd (1978)
11. Mott, N.T.: A theory of the origin of fatigue cracks. Acta Metall. **6**, 195–197 (1958)
12. Boettner, R.C., McEvily, A.J., Liu, Y.C.: On the Formation of fatigue crack. Phil. Mag. **10**, 95 (1964)
13. Yokobori, T., Kawasaki, T., Nakanishi, S., Kawaghishi, M.: Some experiments on heavy section specimen under low-cycle fatigue testing. Met. Sci. J. **5**(1), 25–33 (1969)
14. McEvily, A.J., Johnston, T. L.: International Conference on Fracture, Sendai (1965)
15. Forsyth, P.J.E.: Fatigue damage and crack growth in aluminum alloys. Acta Metall. **11**, 713 (1963)
16. Liaw, P.K., Saxena, A., Schaffer, J.: Creep crack growth behaviour of steam pipe steels: effects of inclusion content and primary creep. Eng. Fract. Mech. **57**(1), 112 (1997)
17. Mills, W.J., James, L.A.: Effect of temperature on the fatigue crack propagation behaviour of inconel X-750. Fatigue Eng. Mater. struct. **3**, 172 (1980)
18. Metals Handbook: Failure Analysis and Prevention, vol. **10**, 8th edn. ASM 102 (1975)
19. Rice, R.C., Rungta, R.: Fatigue analysis of a rail subjected to controlled service conditions. Fatigue Fract. Eng. Mater. Struct. **10**(3), 213–221 (1987)
20. Schijve, J.: Fatigue of Structures and Materials. Kluwer Academic Publisher, Dordrecht 36 (2004)
21. Metals Handbook: Fractography, vol. **12**, 9th Edn. ASM, p. 483 (1987)
22. Metals Handbook: Failure Analysis and Prevention, vol. **10**, 8th edn. ASM, p. 97 (1975)
23. Metals Handbook: Failure Analysis and Prevention, vol. **10**, 8th edn. ASM, p. 100 (1975)
24. Metals Handbook: Failure Analysis and Prevention, vol. **10**, 8th edn. ASM, p. 275 (1975)
25. Frost, N.E., Marsh, K.J., Pook, L.P.: Metal Fatigue. Clarendon, Oxford (1974)
26. Hutchings, F.R., Unterweiser, P.M. (Ed.): Fatigue failure of a diesel engine Crankshaft, from Failure Analysis the British Engine Technical Reports. ASM (1981)
27. Wulpi, D.J.: Understanding How Components Fail, 2nd ed., ASM (1986)
28. Thompson, N., Wadsworth, N.J.: Metal fatigue. Adv. Phys. **7**(25), 72 (1958)
29. Nine, H.D., Kuhlmann-Wilsdorf, D.: Fatigue in copper single crystals in a new model of fatigue in face-centered-cubic metals. Can. J. Phys. **45**(2), 865 (1967)
30. Schijve, J.: Fatigue of Structures and Materials. Kluwer Academic Publisher, Dordrecht 30 (2004). 30
31. Laird, C.: The influence of metallurgical structures on the mechanism of fatigue crack propagation. FORD Scientific Laboratory, Dearborn (1966)
32. Davidson, D.L., Lankford, J.: Fatigue crack growth in metals and alloys. Mechanisms and Micromechanics, International Materials Review. **37**, 45–76 (1992)
33. Grinberg N.: stage II fatigue crack growth. Int. J. Fract. **3**, 143 (1981)
34. Grinberg N.M.: stage II fatigue crack growth Int. J. Fract. **6**, 143–148 (1984)

35. Beachem C.D.: Microscopic fracture processes in Fracture an Advanced Treatise In: Liebowitz H. (ed.). Trans ASM **60**, 311 (1968)
36. Gross T.S.: Micro mechanisms of monotonic and cyclic crack growth. Metals Handbook, vol. **19**, Fatigue and Fracture, ASM (1996)
37. Forsyth, P.J.E.: Fatigue damage and crack growth in aluminum alloys. Acta Metall. **11**, 708 (1963)
38. Forsyth P.J.E., Stubbington G.A., Clark D.: Brittle Striations. J. Inst. Met. **90**, 238–239 (1961)
39. Beachem, C.D., Pelloux, M.N.: Electron fractography: a tool for the study of micromechanisms of fracturing processes. 67th ASTM Symposium, STP-381, 236–237 (1964)
40. Beachem, C.D: Transactions AMS **60**, 325 (1967)
41. Becker, W.: Closed-form modeling of the unloaded mode I dugdale crack. Eng. Fract. Mech. **57**(4), 355–364 (1997)
42. Nelson, H.G.: Hydrogen embrittlement. Treatise on materials science and technology, vol. **25**, 331, Academic, New york (1983)
43. Forsyth, P.J.E., Ryder, D.A.: Some results of the examination of aluminum alloy specimen fracture surfaces. Acta Metall. **63**, 117–124 (1961)
44. Pelloux, R.M., Faral, M., McGee, W.M.: Fractographic measurements of crack-tip closure. ASTM-STP **700**, 35–48 (1980)
45. Srivatsan, T.S., Shiram, S., Daniels, C.: Influence of temperature on cyclic stress response and fracture behavior of aluminum alloy 6061. Eng. Fract. Mech. **56**(4), 536 (1997)
46. Pelloux, R.M.N.: Corrosion fatigue crack propagation. II International Conference on Fracture, Brighton, Session V, Paper 64 (1969)
47. Pelloux, R.M.N.: Mechanisms of formation of striations. Trans. ASM **62**, 281–284 (1969)
48. McClintoc, F.A., Pelloux, R.M.N.: Crack extension by alternating shear. Boeing Scientific Research Laboratories D-1 (1968)
49. Leger, J.: Fatigue life testing of crane drive shaft under crane-typical torsional and rotary bending loads. Schenck Hydropuls Mag. **1**(89), 8–11 (1989)